

Yb₅Ga₂Sb₆: A Mixed Valent and Narrow-Band Gap Material in the RE₅M₂X₆ Family

Udumula Subbarao,[†] Sumanta Sarkar,[†] Vijay Kumar Gudelli,[‡] V. Kanchana,[‡] G. Vaitheeswaran,[§] and Sebastian C. Peter^{*,†}

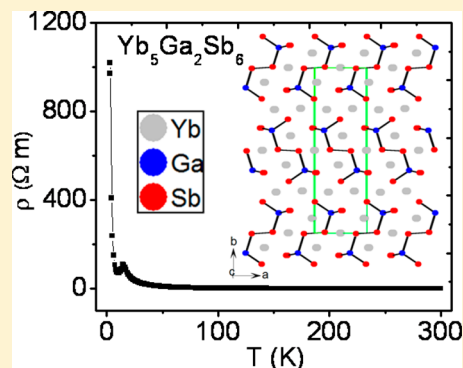
[†]New Chemistry Unit, Jawaharlal Nehru Centre for Advanced Scientific Research, Jakkur, Bangalore, 560064, India

[‡]Department of Physics, Indian Institute of Technology Hyderabad, Ordnance Factory Estate, Yeddumailaram 502 205, Andhra Pradesh, India

[§]Advanced Centre of Research in High Energy Materials (ACRHEM), University of Hyderabad, Prof. C. R. Rao Road, Gachibowli, Hyderabad-500046, Andhra Pradesh, India

S Supporting Information

ABSTRACT: A new compound Yb₅Ga₂Sb₆ was synthesized by the metal flux technique as well as high frequency induction heating. Yb₅Ga₂Sb₆ crystallizes in the orthorhombic space group *Pbam* (no. 55), in the Ba₅Al₂Bi₆ structure type, with a unit cell of $a = 7.2769(2)$ Å, $b = 22.9102(5)$ Å, $c = 4.3984(14)$ Å, and $Z = 2$. Yb₅Ga₂Sb₆ has an anisotropic structure with infinite anionic double chains (Ga₂Sb₆)¹⁰⁻ cross-linked by Yb²⁺ and Yb³⁺ ions. Each single chain is made of corner-sharing GaSb₄ tetrahedra. Two such chains are bridged by Sb₂ groups to form double chains of $1/\infty$ [Ga₂Sb₆¹⁰⁻]. The compound satisfies the classical Zintl–Klemm concept and is a narrow band gap semiconductor with an energy gap of around 0.36 eV calculated from the electrical resistivity data corroborating with the experimental absorption studies in the IR region (0.3 eV). Magnetic measurements suggest Yb atoms in Yb₅Ga₂Sb₆ exist in the mixed valent state. Temperature dependent magnetic susceptibility data follows the Curie–Weiss behavior above 100 K and no magnetic ordering was observed down to 2 K. Experiments are accompanied by all electron full-potential linear augmented plane wave (FP-LAPW) calculations based on density functional theory to calculate the electronic structure and density of states. The calculated band structure shows a weak overlap of valence band and conduction band resulting in a pseudo gap in the density of states revealing semimetallic character.



1. INTRODUCTION

Zintl phases are special class of intermetallic compounds comprised of a highly electropositive metal ion and a polyanionic network.¹ These compounds have drawn much attention because of their applications in the field of thermoelectrics. The reason behind this fascinating behavior stems from their “dual nature”, i.e., they can act as both crystal and glass. Because of this ability, Zintl phases generally show high electrical conductivity (like crystal) and low thermal conductivity (like glass).^{2–6} Zintl phases containing heavier p-block elements usually exhibit a narrow band gap; e.g., Ba₈In₄Sb₁₆⁷ and BaGa₂Sb₂⁸ are found to be narrow band gap p-type semiconductors. This in turn facilitates the transfer of electrons from the valence band to the conduction band. The presence of heavier elements (e.g., Sb, Bi, and alkaline/rare earth elements) also enhances the phonon scattering due to soft binding⁹ and hence the lattice contribution (k_{Lattice}) toward overall thermal conductivity decreases which effectively results in a higher ZT value.

Compounds with general formula Ae₅Tr₂Pn₆ (Ae = Ca, Sr, Ba; Tr = Al, Ga, In; Pn = As, Sb, Bi) are classified as the Zintl phase. Though these compounds were studied for their

structural and basic physical properties for decades,^{10–15} their potential ability as thermoelectric materials was understood very recently.^{10–16} These compounds crystallize in two different types of structures, namely, Ca₅Ga₂As₆^{14,17} and Ba₅Al₂Bi₆.^{11,13,18} Both structures contain basic MPn₄ tetrahedra sharing their corners and are bridged by Pn₂ dumbbells forming infinite parallel ladders; however, the orientation of these ladder like geometries differ in these two structures. Ca₅Al₂Sb₆ was the first member to be investigated as thermoelectric material by Toberer et al.¹⁹ Their report spurred a series of studies in the succeeding years dealing with the thermoelectric properties and other related studies like transport, optical properties, and band structure calculations on the analogous compounds.^{20–25} Yan et al. reported the first-principle calculations of the electronic structure and the transport coefficient of Ca₅Al₂Sb₆ at different temperatures. The carrier concentrations²⁰ and the anisotropic one-dimensional structure of Ca₅Ga₂As₆ are favorable for a good thermoelectric material with thermoelectric figure of merit ZT of 0.7 at 930 K.²¹ Later, the compounds Zn-doped

Received: August 27, 2013

Published: November 13, 2013

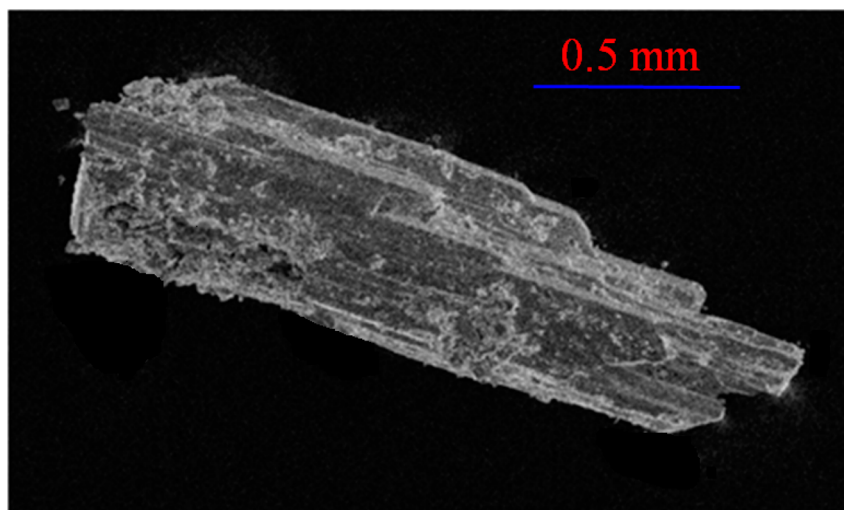


Figure 1. Typical SEM image of Yb₅Ga₂Sb₆ single crystal grown from the active Ga flux.

Ca₅Al₂Sb₆,²² Mn doped Ca₅Al₂Sb₆ and Ca₅M₂Sb₆ (M = Al, Ga, and In),²³ and Ca₅M₂Sb₆ (M = Al, Ga, and In)^{24,25} were also studied for the thermoelectric properties.

Interestingly, only three rare earth based compounds in the RE₅M₂X₆ family were reported: one Eu based compound, Eu₅In₂Sb₆, and two Yb based compounds, Yb₅Al₂Sb₆^{26,27} and Yb₅In₂Sb₆.¹⁵ Eu₅In₂Sb₆ crystallizes in the Ca₅Ga₂As₆ type structure, while the two Yb compounds crystallize in the Ba₅Al₂Bi₆ type structure. The three compounds were studied for detailed crystallography, electrical conductivity, thermo power, and thermal conductivity. Band structure calculations performed on these three compounds confirmed the presence of the narrow/zero band gap. It is a well-established fact that Eu and Yb can exist in divalent and trivalent states due to the presence of an unstable electronic 4f-shell, as they show two electronic configurations that are closely spaced in energy: for Eu, the magnetic Eu²⁺(4f⁷) and nonmagnetic Eu³⁺(4f⁶), and for Yb, the magnetic Yb³⁺(4f¹³) and nonmagnetic Yb²⁺(4f¹⁴). However, in all three compounds the rare earths were assigned as divalent according to the Zintl–Klemm concept.

Here, we report a new compound Yb₅Ga₂Sb₆ obtained from the metal flux method. To the best of our knowledge, this compound is the first Ga-containing member in the RE₅M₂X₆ family. Yb₅Ga₂Sb₆ crystallizes in the orthorhombic Ba₅Al₂Bi₆ structure type with the space group of *Pbam* (no. 55). Temperature dependent magnetic susceptibility data reveals that Yb in this compound exists in the mixed valent state with around 58% of Yb in the trivalent state. The overall electrical resistivity curve is reminiscent of a semimetallic behavior. The band gap calculated from the resistivity data was 0.36 eV hinting toward a narrow band gap semiconductor and is well corroborated with the band structure calculations and absorption studies.

2. EXPERIMENTAL SECTION

2.1. Synthesis. The following reagents were used as purchased without further purification: Yb (in the form of metal pieces cut from metal chunk, 99.99%, Alfa Aesar), Ga (pieces, 99.999%, Alfa Aesar), and Sb (shots, 99.99%, Alfa-Aesar).

2.1.1. Metal Flux Method. Well shaped single crystals of Yb₅Ga₂Sb₆ were obtained by combining ytterbium metal (0.3 g), gallium pieces (2 g), and antimony shots (0.4 g) in an alumina crucible. The crucible was placed in a 13 mm fused silica tube which was flame-sealed under

a vacuum of 10⁻⁵ Torr to prevent oxidation during heating. The reactants were then heated to 1273 K over 10 h, maintained at that temperature for 5 h to allow proper homogenization, then cooled down to 1123 K in 2 h, and kept at this temperature for 72 h. Finally, the sample was allowed to cool slowly to 303 K over 48 h. No reactions with the alumina crucible material was detected. The reaction product was isolated from the excess gallium flux by heating at 673 K and subsequently centrifuging through a coarse frit. Extra gallium was removed by immersion and sonication in 2–4 M solution of iodine in dimethylformamide (DMF) over 12–24 h at room temperature. The product was rinsed with hot water and DMF and dried with acetone and ether. The gray crystals of Yb₅Ga₂Sb₆ are large (1 mm) and rodlike obtained in high yield (>90%). A very small amount of Ga metal present in the product was quite unavoidable (detected in powder XRD). Yb₅Ga₂Sb₆ is stable in air and no decomposition was observed even after several months. Several crystals, which grow as metallic silver rods, were carefully selected for the elemental analysis.

2.1.2. High-Frequency Induction Heating Method. Ytterbium, gallium, and antimony were mixed in the ideal 5:2:6 atomic ratio and sealed in a tantalum ampule under argon atmosphere in an arc-melting apparatus. The tantalum ampule was subsequently placed in a water-cooled sample chamber of an induction furnace (Easy Heat induction heating system, model 7590), first rapidly heated to 180 Amperes (~1200–1350 K) and kept at that temperature for 30 min. Finally the reaction was rapidly cooled to room temperature by switching off the power supply. All compounds could easily be removed from the tantalum tubes. No reactions with the crucible could be detected. The compound was found to be stable in ambient aerial conditions for several months. The samples were in polycrystalline form and light gray in color. The weight loss of the final material was found to be less than 1%. The samples obtained from the high frequency induction heating method were used for the property studies.

2.2. Elemental Analysis. Semiquantitative microanalyses were performed on the single crystals obtained from the flux techniques using a Leica 220i scanning electron microscope (SEM) equipped with a Bruker 129 eV energy dispersive X-ray analyzer (EDS). Data were acquired with an accelerating voltage of 20 kV and 90 s accumulation time. SEM image of a typical single crystal of Yb₅Ga₂Sb₆ is shown in Figure 1. The EDS analyses were performed on visibly clean surfaces of the single crystals obtained from the flux method indicated that the atomic composition was close to 5:2:6, which is in good agreement with the composition obtained from the single crystal X-ray data refinement.

2.3. Powder X-ray Diffraction. Phase identity and purity of the Yb₅Ga₂Sb₆ sample were determined by powder XRD experiments that were carried out with a Bruker D8 Discover diffractometer using Cu-K α radiation ($\lambda = 1.5406 \text{ \AA}$). The experimental powder pattern of

$\text{Yb}_3\text{Ga}_2\text{Sb}_6$ was found to be in good agreement with the pattern calculated from the single-crystal X-ray structure refinement.

2.4. Single Crystal X-ray Diffraction. X-ray diffraction data was collected on a selected single crystal of $\text{Yb}_3\text{Ga}_2\text{Sb}_6$ at room temperature using a Bruker Smart Apex 2-CCD diffractometer equipped with a normal focus, 2.4 kW sealed tube X-ray source with graphite monochromatic Mo-K α radiation ($\lambda = 0.71073 \text{ \AA}$) operating at 50 kV and 30 mA, with ω scan mode. A crystal of suitable size ($0.5 \times 0.05 \times 0.05 \text{ mm}^3$) was cut from a plate shaped crystal and mounted on a thin glass ($\sim 0.1 \text{ mm}$) fiber with commercially available super glue. A full sphere of 60 frames was acquired up to 73.28° in 2θ . The individual frames were measured with steps of 0.50° and an exposure time of 10 s per frame. The program SAINT²⁸ was used for integration of diffraction profiles, and absorption correction were made with the SADABS program.²⁹ The systematic absences led to the non-centrosymmetric space group *Pbam*. However, the Platon program with WinGx system, ver. 1.80.05³⁰ was used to check the additional symmetry and confirms the final structure refinement. The structure was solved by SHELXS 97³¹ and refined by a full matrix least-squares method using SHELXL³² with anisotropic atomic displacement parameters for all atoms. Packing diagrams were generated with Diamond.³³ As a check for the correct composition, the occupancy parameters were refined in a separate series of least-squares cycles. All bond lengths are within the acceptable range compared to the theoretical values. Details of the crystallographic data are given in Tables 1–4.

2.5. Magnetic Measurements. Magnetic measurements were carried out using a Quantum Design MPMS-SQUID magnetometer. Measurements were performed on polycrystalline sample, which were ground and screened by powder XRD to verify phase identity and purity. Temperature dependent data were collected in field cooled mode (FC) between 2 and 300 K in an applied field (H) of 1 tesla (T). Magnetization data were also collected for $\text{Yb}_3\text{Ga}_2\text{Sb}_6$ at 2 and 300 K with field sweeping from -60 to 60 T .

2.6. Electrical Resistivity. The resistivity measurements were performed under an applied field of 1 T on $\text{Yb}_3\text{Ga}_2\text{Sb}_6$ with a conventional ac four probe setup. Four very thin copper wires were glued to the pellet using a strongly conducting silver epoxy paste. The data were collected in the range 3–300 K using a commercial Quantum Design Physical Property Measurement System (QD-PPMS).

2.7. Optical Measurements. Diffuse reflectance measurement on the $\text{Yb}_3\text{Ga}_2\text{Sb}_6$ compound was performed with a Bruker IFS 66v/s instrument by the KBr pellet method in the mid-IR and NIR spectral ranges. The polycrystalline sample obtained from the high frequency induction heating was used for the measurement.

2.8. Computational Details. To study the electronic properties we have used the full-potential linear augmented plane wave (FP-LAPW) method based on first-principle density functional calculations as implemented in the WIEN2k which yield reliable results for the electronic and structural properties of crystalline solids.³⁴ The calculations are carried out by solving the Kohn–Sham equations self-consistently based on the Generalized Gradient Approximation of Perdew–Burke–Ernzerhof (GGA-PBE) scheme for the exchange–correlation potential.³⁵ The muffin-tin radii were chosen as 2.5 au for Yb and 2.3 au for both Ga and Sb atoms. To achieve the convergence of energy eigenvalues, the wave functions in the interstitial region were expanded using plane waves with a cutoff of $R_{\text{MT}}K_{\text{max}} = 11$, where K_{max} is the plane wave cutoff, and R_{MT} is the smallest of all atomic sphere radii. The charge density was Fourier expanded up to $G_{\text{max}} = 12$. The maximum value for the wave function expansion inside the atomic spheres was confined to $l_{\text{max}} = 10$. Convergence tests were carried out using higher G_{max} and $R_{\text{MT}}K_{\text{max}}$ values, giving no significant changes in the calculated properties. Here we have used 1000 k-points for $\text{Yb}_3\text{Ga}_2\text{Sb}_6$ k-mesh in the Monkhorst–Pack scheme,³⁶ resulting in 154 k-points in the irreducible part of the Brillouin zone for the self-consistent calculation with the inclusion of spin–orbit coupling. All our calculations are performed with the experimental parameters with an energy convergence up to 10^{-6} Ry between the successive iterations per unit cell.

3. RESULTS AND DISCUSSION

3.1. Structure Refinement. The crystal structure of $\text{Yb}_3\text{Ga}_2\text{Sb}_6$ was refined using SHELXL-97 (full-matrix least-squares on F^2) with anisotropic atomic displacement parameters for all atoms. As a check for the correct composition, the occupancy parameters were refined in a separate series of least-squares cycles. Single crystals of $\text{Yb}_3\text{Ga}_2\text{Sb}_6$ from different syntheses batches were used for the data collection. The lattice parameters of the $\text{Ca}_3\text{Al}_2\text{Bi}_6$ structure were taken at the initial step and the refinement resulted in seven crystallographic positions in the $\text{Yb}_3\text{Ga}_2\text{Sb}_6$ structure; one ytterbium atom occupies the $2a$ site, two ytterbium atoms occupy the $4g$ sites, one gallium atom occupies the $4h$ site, and three antimony atoms occupy the $4h$, $4h$, and $4g$ sites.

The data collection and structure refinement for $\text{Yb}_3\text{Ga}_2\text{Sb}_6$ are listed in Table 1. The standard atomic positions and

Table 1. Crystal Data and Structure Refinement for $\text{Yb}_3\text{Ga}_2\text{Sb}_6$ at 296(2) K^a

empirical formula	$\text{Yb}_3\text{Ga}_2\text{Sb}_6$
formula weight	1735.14
temperature	296(2) K
wavelength	0.71073 Å
crystal system	orthorhombic
space group	<i>Pbam</i>
unit cell dimensions	$a = 7.2769(2) \text{ \AA}$ $b = 22.9102(5) \text{ \AA}$ $c = 4.39840(10) \text{ \AA}$
volume	$733.28(3) \text{ \AA}^3$
Z	2
density (calculated)	7.859 g/cm^3
absorption coefficient	45.936 mm^{-1}
$F(000)$	1436
crystal size	$0.10 \times 0.05 \times 0.05 \text{ mm}^3$
θ range for data collection	1.78 to 48.01°
index ranges	$-15 \leq h \leq 15$, $-47 \leq k \leq 47$, $-4 \leq l \leq 9$
reflections collected	24 672
independent reflections	3799 [$R_{\text{int}} = 0.0584$]
completeness to $\theta = 48.01^\circ$	99.9%
refinement method	full-matrix least-squares on F^2
data/restraints/parameters	3799/0/42
goodness-of-fit	1.062
final R indices [$>2\sigma(I)$]	$R_{\text{obs}} = 0.0329$, $wR_{\text{obs}} = 0.0796$
R indices [all data]	$R_{\text{all}} = 0.0384$, $wR_{\text{all}} = 0.0827$
extinction coefficient	0.0013(1)
largest diff. peak and hole	8.208 and $-3.461 \text{ e \AA}^{-3}$

^a $R = \sum |F_o| - |F_c| / \sum |F_o|$, $wR = \{ \sum [w(|F_o|^2 - |F_c|^2)^2] / \sum [w(|F_o|^4)] \}^{1/2}$ and calc $w = 1 / [\sigma^2(F_o^2) + (0.0359P)^2 + 6.1794P]$ where $P = (F_o^2 + 2F_c^2) / 3$.

isotropic atomic displacement parameters of this compound are collected in Table 2. The anisotropic displacement parameters and important bond lengths are listed in Tables 3 and 4, respectively. Further information on the structure refinements is available from Fachinformationszentrum Karlsruhe, D-76344 Eggenstein-Leopoldshafen (Germany) by quoting the Registry No. CSD-426568

3.3. Crystal Chemistry. The compound $\text{Yb}_3\text{Ga}_2\text{Sb}_6$ crystallizes in the orthorhombic the $\text{Ba}_3\text{Al}_2\text{Bi}_6$ ^{11,13,18} structure type, *Pbam* space group, lattice parameters $a = 7.2769(2) \text{ \AA}$, $b = 22.9102(5) \text{ \AA}$, and $c = 4.3984(1) \text{ \AA}$. $\text{Yb}_3\text{Al}_2\text{Sb}_6$ ^{26,27} and

Table 2. Atomic Coordinates ($\times 10^4$) and Equivalent Isotropic Displacement Parameters ($\text{\AA}^2 \times 10^3$) for $\text{Yb}_5\text{Ga}_2\text{Sb}_6$ at 296(2) K with Estimated Standard Deviations in Parentheses^a

label	Wyckoff site	x	y	z	occupancy	U_{eq}^a
Yb1	2a	9578(1)	884(1)	5000	1	11(1)
Yb2	4g	2663(1)	2465(1)	5000	1	10(1)
Yb3	4g	5000	0	5000	1	10(1)
Ga	4h	3163(1)	1218(1)	0	1	12(1)
Sb1	4h	5288(1)	1358(1)	5000	1	9(1)
Sb2	4h	90(1)	1880(1)	0	1	9(1)
Sb3	4g	2004(1)	10046(1)	0	1	10(1)

^a U_{eq} is defined as one-third of the trace of the orthogonalized U_{ij} tensor.

Table 3. Anisotropic Displacement Parameters ($\text{\AA}^2 \times 10^3$) for $\text{Yb}_5\text{Ga}_2\text{Sb}_6$ at 296(2) K with Estimated Standard Deviations in Parentheses^a

label	U_{11}	U_{22}	U_{33}	U_{12}	U_{13}	U_{23}
Yb1	12(1)	9(1)	12(1)	-1(1)	0	0
Yb2	5(1)	10(1)	14(1)	0(1)	0	0
Yb3	6(1)	10(1)	14(1)	-1(1)	0	0
Ga	8(1)	14(1)	13(1)	0(1)	0	0
Sb1	6(1)	7(1)	14(1)	0(1)	0	0
Sb2	8(1)	11(1)	9(1)	2(1)	0	0
Sb3	7(1)	12(1)	11(1)	-1(1)	0	0

^aThe anisotropic displacement factor exponent takes the form: $-2\pi^2[h^2a^2U_{11} + \dots + 2hkabU_{12}]$.

Table 4. Selected Bond Lengths [\AA] for $\text{Yb}_5\text{Ga}_2\text{Sb}_6$ at 296(2) K with Estimated Standard Deviations in Parentheses

label	distances	label	distances	label	distances
Yb1–Yb1	4.0953(5)	Yb1–Sb3	3.2711(3)	Yb3–Sb3	3.0988(2)
Yb1–Yb2	4.0319(3)	Yb1–Sb3	3.4106(3)	Yb1–Ga	3.4968(5)
Yb1–Yb2	4.2619(3)	Yb2–Sb1	3.1751(4)	Yb2–Ga	3.6236(6)
Yb1–Yb3	3.8982(3)	Yb2–Sb1	3.2036(4)	Sb1–Ga	2.7074(4)
Yb2–Yb2	3.6420(1)	Yb2–Sb2	3.1845(4)	Sb2–Ga	2.7017(7)
Yb1–Sb1	3.3056(4)	Yb2–Sb2	3.1953(3)	Sb3–Ga	2.8136(8)
Yb1–Sb2	3.1909(3)	Yb3–Sb1	3.1178(3)	Sb3–Sb3	2.9235(7)

$\text{Yb}_5\text{In}_2\text{Sb}_6$ ¹⁵ are the two other Yb based compounds reported in the $\text{Ba}_5\text{Al}_2\text{Bi}_6$ type structure and a detailed crystal structure description is reported elsewhere. Nevertheless, here we briefly explain the important features in the crystal structure of $\text{Yb}_5\text{Ga}_2\text{Sb}_6$ and compared with those reported systems. The crystal structure of $\text{Yb}_5\text{Ga}_2\text{Sb}_6$ along the [001] direction is shown in Figure 2. As reported, the crystal structure of $\text{Yb}_5\text{Ga}_2\text{Sb}_6$ can be explained as composition of infinite one-dimensional $[\text{Ga}_2\text{Sb}_6]^{10-}$ double chains arranged in parallel fashion in the [110] plane resulting in the formation of a stable crystal structure. These double chains are interconnected by GaSb_4 tetrahedral single chains bridged by Sb_2 dumbbell groups shown in Figures 2 and 3. The next layer of double chains, below the ab plane, is crystallographically equivalent and related by b -glide and a -glide symmetry operations perpendicular to the a and b directions and are separated by Yb cations, respectively (Figure 2). The Yb atoms situated between the rows of infinite $[\text{Ga}_2\text{Sb}_6]^{10-}$ play crucial roles in providing charge balance and effective Coulomb screening. On the basis of the Zintl–Klemm concept, the formula for the compounds

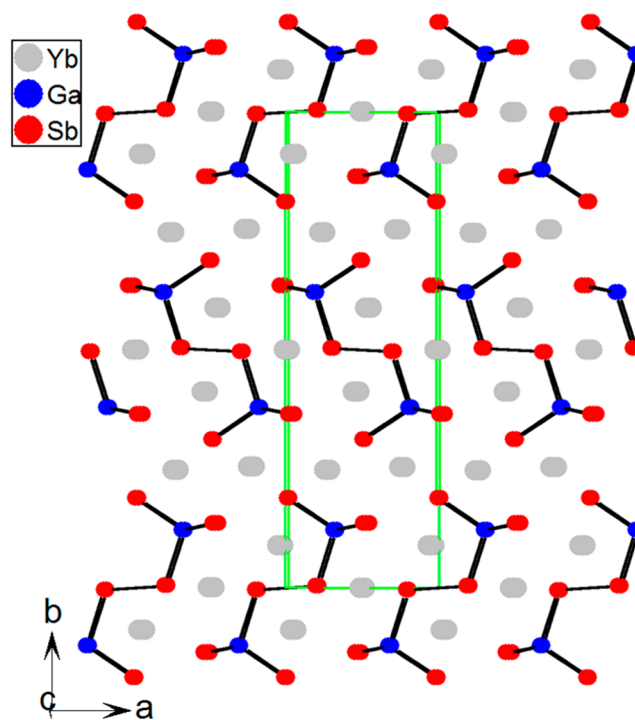


Figure 2. Crystal structure of $\text{Yb}_5\text{Ga}_2\text{Sb}_6$ as viewed along the [001] axis; the unit cell is outlined as green solid lines.

$\text{Yb}_3\text{Al}_2\text{Sb}_6$ ^{26,27} and $\text{Yb}_3\text{In}_2\text{Sb}_6$ ¹⁵ have been proposed as $(\text{Yb}^{2+})_3[(\{\text{Al/In}\}^{3+})_2(\text{Sb}_2^{4-})(\text{Sb}^{3-})_4]$.^{15,26} However, our magnetic measurements on the selected single crystals of $\text{Yb}_5\text{Ga}_2\text{Sb}_6$ indicate mixed valent behavior of Yb (discussed below).

For a close investigation on the Yb valence, the coordination environment of three Yb atoms are drawn and shown in Figure 4 as similar to the previous reports of $\text{Yb}_3\text{Al}_2\text{Sb}_6$ and $\text{Yb}_3\text{In}_2\text{Sb}_6$. The coordination environments of Yb in $\text{Yb}_5\text{Ga}_2\text{Sb}_6$ exactly matches with the compounds $\text{Yb}_3\text{Al}_2\text{Sb}_6$ ^{26,27} and $\text{Yb}_3\text{In}_2\text{Sb}_6$,¹⁵ and all the bonding and structural explanations remain the same in the new compound as well. The average bond distances between Yb and Sb atoms within the first coordination sphere for all three Yb atoms were calculated and found in the order Yb1–Sb (3.2929 \AA) > Yb2–Sb (3.1897 \AA) > Yb3–Sb (3.0988 \AA). Considering the fact that divalent Yb is larger in size (1.86 \AA)^{37,38} compared to trivalent Yb (1.66 \AA),^{37,38} Yb1 can be in the divalent state (Wyckoff site 2a, 20%), Yb2 in the mixed valent state (Wyckoff site 4g, 20% divalent and 20% trivalent), and Yb3 in the trivalent state (Wyckoff site 4g, 40%) bearing the ratio of trivalent Yb to divalent Yb as 60:40. Finally, assuming the mixed valent state of ytterbium as per our magnetic studies and crystal structure, the formula for the compound $\text{Yb}_5\text{Ga}_2\text{Sb}_6$ can be described as $(\text{Yb}^{3+})_3(\text{Yb}^{2+})_2[(\text{Ga}^{1-})_2(\text{Sb}^{1-})_1(\text{Sb}^{2-})_5]$ or alternatively $(\text{Yb}^{3+})_3(\text{Yb}^{2+})_2[(\text{Ga}^{3+})_2(\text{Sb}^{3-})_5(\text{Sb}^{4-})_1]$. Similar differences in the Yb–Sb bond distances for all three Yb atoms in the $\text{Yb}_3\text{Al}_2\text{Sb}_6$ and $\text{Yb}_3\text{In}_2\text{Sb}_6$ structures were also found. A detailed magnetic susceptibility and X-ray absorption near edge spectroscopy (XANES) measurement will be performed in the near future on all compounds to understand the valence state of rare earths and other atoms.

3.4. Physical Properties. **3.4.1. Magnetism.** Magnetic susceptibility measurements were performed on polycrystalline sample of $\text{Yb}_5\text{Ga}_2\text{Sb}_6$ obtained from the high frequency

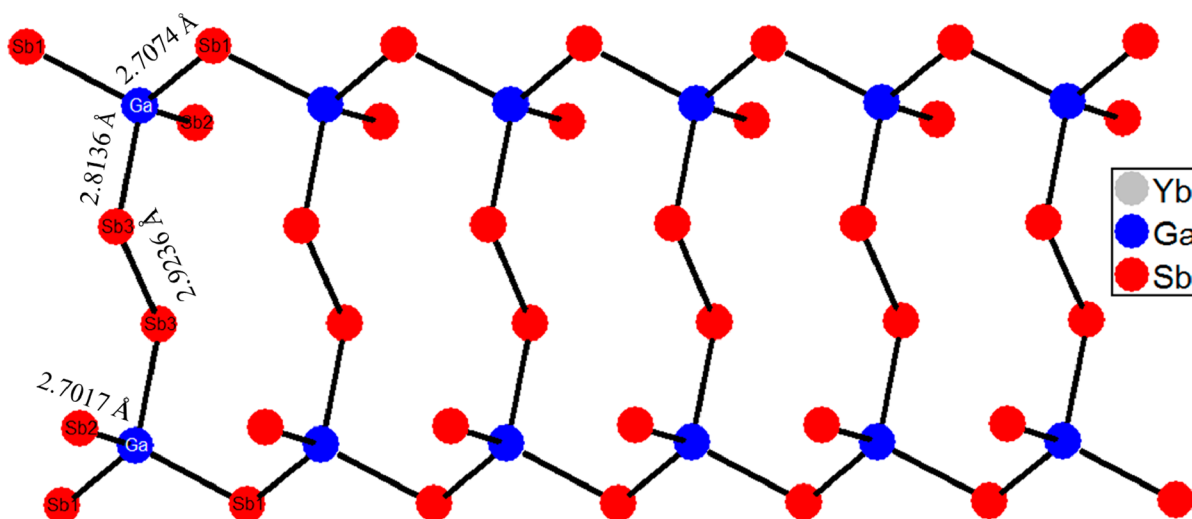


Figure 3. $1/\infty [\text{Ga}_2\text{Sb}_6]^{13-}$ double chains with atomic labeling and bond lengths. The ladder type structures of double chains are tetrahedral bridged by Sb–Sb bonding.

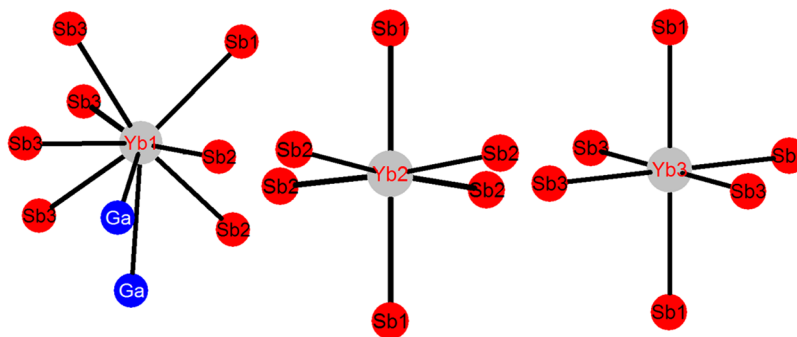


Figure 4. Coordination environment of Yb1, Yb2, and Yb3 atoms in $\text{Yb}_5\text{Ga}_2\text{Sb}_6$.

induction heating synthesis. The temperature dependent molar magnetic susceptibility (χ_m) and inverse susceptibility ($1/\chi_m$) of $\text{Yb}_5\text{Ga}_2\text{Sb}_6$ at an applied field of 1 T are shown in Figure 5. The

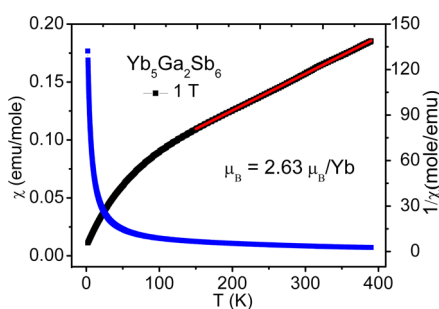


Figure 5. Temperature dependent magnetic susceptibility (χ_m) and inverse magnetic susceptibility ($1/\chi_m$) of $\text{Yb}_5\text{Ga}_2\text{Sb}_6$.

inverse susceptibility curve above 150 K for $\text{Yb}_5\text{Ga}_2\text{Sb}_6$ obeys Curie–Weiss law, $\chi(T) = C/(T - \theta)$,^{39,40} where C is the Curie–Weiss constant ($N_A\mu_{\text{eff}}^2/3k_B T$) and θ_p is the Weiss temperature. A fit to the curve above 150 K resulted in an effective magnetic moment (μ_{eff}) of $2.63 \mu_B/\text{Yb}$ atom suggesting the existence of mixed valency in Yb atoms of $\text{Yb}_5\text{Ga}_2\text{Sb}_6$. The estimated experimental μ_{eff} value is about 58% of that expected for a free ion Yb^{3+} moment ($4.56 \mu_B/\text{Yb}$). Temperature dependent magnetic susceptibility data of $\text{Yb}_5\text{Ga}_2\text{Sb}_6$ shows no magnetic ordering down to 2 K but the

susceptibility slightly increases at lower temperature which is normal for rare earth based intermetallics.^{41–48} This lower temperature deviation can be attributed to crystal field contributions and/or to a possible onset of valence fluctuations.

The field dependence of the magnetization $M(H)$ for ground samples of $\text{Yb}_5\text{Ga}_2\text{Sb}_6$ were measured at 2 and 300 K shown in Figure 6. The data measured at 300 K exhibit linear behavior and no signs of saturation up to our highest attainable field of 60 T. The magnetization curve taken at 2 K shows a slight field dependent response up to ~ 30 T and continues to rise slowly up to the highest obtainable field (60 T) without any hint of saturation.

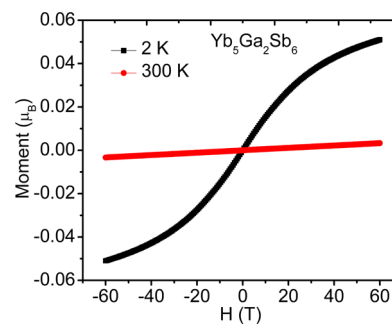


Figure 6. Magnetization as a function of applied magnetic field at 2 and 300 K for the polycrystalline sample of $\text{Yb}_5\text{Ga}_2\text{Sb}_6$.

3.4.2. Electrical Resistivity. The electrical resistivity of polycrystalline $\text{Yb}_5\text{Ga}_2\text{Sb}_6$ sample obtained from the high frequency induction heating is shown in Figure 7. Resistivity

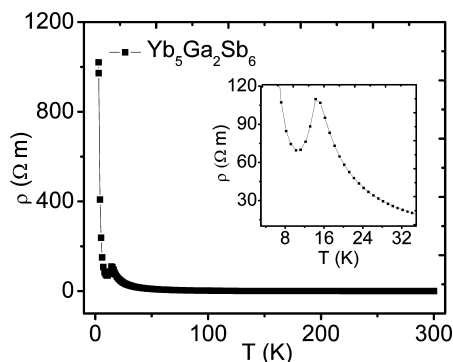


Figure 7. Resistivity (ρ) measured as a function of temperature. Inset shows that there is a transition at 15 K.

does not vary much with temperature down to 35 K. Below this temperature, resistivity increases exponentially and starts falling following a maximum at around 14 K and a broad minimum at around 10 K. This kind of minima in the resistivity plot is characteristic of the compounds with either a gap/pseudo gap (for semiconductors)⁴⁹ or a Kondo lattice (in case of dilute magnetic alloys).⁵⁰ The decrease in resistivity is an indication of movement of carriers from the valence to conduction band.¹⁹ After the dip, the resistivity increases steeply with temperature which could be attributed to a significant rise in electron–phonon scattering which lowers the carrier mobility. The exponential of the resistivity data is plotted against the inverse temperature and the high temperature end was fitted with the Arrhenius equation $\rho = \rho_0 \exp(E_g/2kT)$ (Figure 8). The fitting

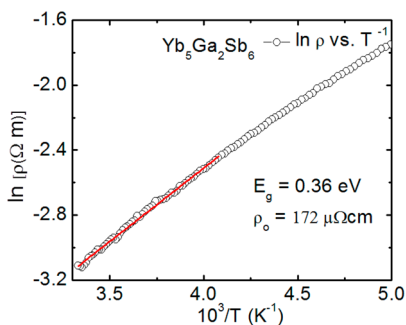


Figure 8. Logarithmic resistivity ($\ln \rho$) vs inverse temperature of $\text{Yb}_5\text{Ga}_2\text{Sb}_6$.

yielded the band gap (E_g) of 0.36 eV which is comparable with other previously reported compounds in the $\text{RE}_5\text{M}_2\text{X}_6$ family²⁴ indicates that $\text{Yb}_5\text{Ga}_2\text{Sb}_6$ can also be considered as a potential candidate for the thermoelectric applications.

3.4.3. Optical Properties. Optical absorption studies were done on the sample in the IR region (Figure 9). The Kubelka–Munk function $(F(R)\hbar\omega)^2$ was plotted against energy ($\hbar\omega$), and a tangent was drawn at the region near the slope change. The tangent was extrapolated up to the x -axis giving rise to an energy band gap of 0.3 eV. This value is very close to the band gap calculated from the electrical resistivity data (0.36 eV). The energy gap in $\text{Yb}_5\text{Ga}_2\text{Sb}_6$ is slightly shorter than the previously

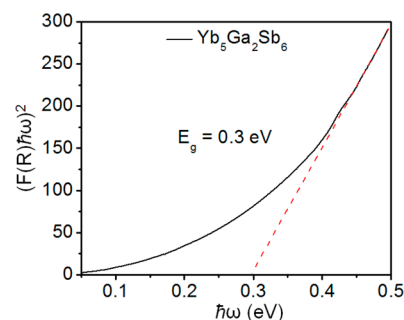


Figure 9. Optical absorption data for $\text{Yb}_5\text{Ga}_2\text{Sb}_6$ plotted in terms of the Kubelka–Munk function against energy (eV). The red dashed lines show a direct band gap of 0.3 eV.

reported compounds $\text{Ca}_5\text{Al}_2\text{Sb}_5$ (0.71 eV), $\text{Ca}_5\text{Ga}_2\text{Sb}_5$ (0.56 eV), and $\text{Ca}_5\text{In}_2\text{Sb}_5$ (0.68 eV).¹⁷

3.4.4. Band Structure and Density of States. Understanding the electronic structure of rare-earth elements and compounds has been a great challenge in the field of condensed matter physics. Several methods have been developed to understand the above from the theoretical perspective. Density functional theory (DFT) is one such methods which is found to be successful in explaining the crystal structure and the complex electronic structure of rare-earth compounds.^{51–53} The major challenge in DFT is toward understanding the complex nature of the rare-earth ion. Standard DFT based exchange–correlations functional are not adequate enough to handle the same and one has to go beyond the standard functionals such as LSDA+U, SIC, and DMFT like approaches. In the present work we have carried out both LDA and LDA+U to investigate the electronic structure of $\text{Yb}_5\text{Ga}_2\text{Sb}_6$ and found no significant differences. The structural parameters of $\text{Yb}_5\text{Ga}_2\text{Sb}_6$ are taken from our experimental results as input for the band structure and density of states calculation. The calculated band structure of $\text{Yb}_5\text{Ga}_2\text{Sb}_6$ including the spin–orbit coupling along the high symmetry directions of the orthorhombic Brillouin zone of the reciprocal space is shown in Figure 10. The band structure of $\text{Yb}_5\text{Ga}_2\text{Sb}_6$ is compared with the isostructural compound $\text{Yb}_5\text{Al}_2\text{Sb}_6$ ²⁶ and we can see both looks similar to each other. The striking feature between the two compounds is in the vicinity of the Fermi level E_F . From Figure 10, we can see a weak overlap of bands near the Fermi level resulting in a semimetallic behavior as seen in other Zintl phase compounds. From the band structure we can see that in the valence band region the bands near -9.0 to -12.0 eV are mainly due to the Sb 5p states. The Ga 3s and Sb 5p states are dominated in the region of -5.5 to 7.0 eV. From 4.5 eV till the Fermi level, the bands are mostly from the Sb 5p states. The conduction band is mainly dominated by the Yb 5d states. A weak hybridization between the conduction and valence band near the Fermi level was observed, which is contributed mainly from the Sb 5p and Yb 5d states. From the density of states it can be clearly seen that the compound has a pronounced pseudogap feature at the Fermi level.

4. CONCLUDING REMARKS

Since the compounds $\text{Yb}_5\text{Al}_2\text{Sb}_6$ and $\text{Yb}_5\text{In}_2\text{Sb}_6$ were already reported in the $\text{RE}_5\text{M}_2\text{X}_6$ family within the $\text{Ba}_5\text{Al}_2\text{Bi}_6$ structure type, the existence of the prototype $\text{Yb}_5\text{Ga}_2\text{Sb}_6$ was highly probable. This motivated us to perform the synthesis of $\text{Yb}_5\text{Ga}_2\text{Sb}_6$ using different synthetic techniques. In the first

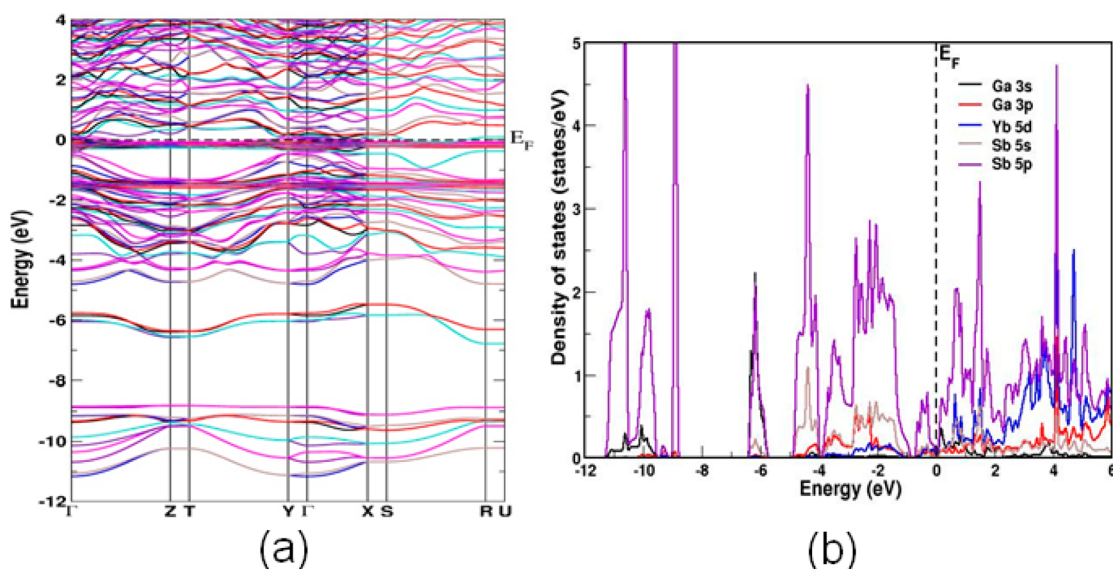


Figure 10. Calculated band structure (a) and projected density of states (b) of $\text{Yb}_5\text{Ga}_2\text{Sb}_6$ within GGA including spin–orbit coupling.

attempt, rod shaped single crystals of $\text{Yb}_5\text{Ga}_2\text{Sb}_6$ were obtained from the metal flux technique using Ga as an active flux. The crystal structure of $\text{Yb}_5\text{Ga}_2\text{Sb}_6$ was studied using the X-ray diffraction data of a good quality single crystal. Later, this compound was also synthesized by a high frequency induction furnace as well. The earlier reports proposed that Yb exists in the divalent state based on the Zintl–Klemm concept. However, our magnetic susceptibility measurements on $\text{Yb}_5\text{Ga}_2\text{Sb}_6$ gave an effective magnetic moment of $2.63 \mu_B/\text{Yb}$ atom, which suggests Yb is in the mixed valent with approximately 58% of Yb^{3+} . Optical measurements and electrical resistivity studies suggest a band gap whereas a pseudogap like feature is seen in the density of states, which is in line with the other compounds in the $\text{RE}_5\text{M}_2\text{X}_6$ family and can be considered as a probable material for the thermoelectric applications. X-ray absorption near edge spectroscopy on all these compounds will be performed in the near future to further confirm the valence state of Yb in these compounds.

■ ASSOCIATED CONTENT

📄 Supporting Information

Crystallographic information file (CIF). This material is available free of charge via the Internet at <http://pubs.acs.org>.

■ AUTHOR INFORMATION

Corresponding Author

*Phone: 080-22082998. Fax: 080-22082627. E-mail: sebastiancp@jncasr.ac.in.

Notes

The authors declare no competing financial interest.

■ ACKNOWLEDGMENTS

We thank JNCASR, Department of Science and Technology, Government of India and Sheikh Saqr Laboratory for the financial support. U.S. and S.S. thank CSIR for the research fellowships, and S.C.P acknowledges the Ramanujan Fellowship from the Department of Science and Technology, Government of India.

■ REFERENCES

- (1) Sevon, S. C. *Zintl Phases in Intermetallic Compounds, Principles and Practice: Progress*; Westbrook, J. H., Freisher, R. L., Eds.; John Wiley & Sons Ltd.: Chichester, England, 2002; p 113.
- (2) Kim, S. J.; Hu, S. Q.; Uher, C.; Hogan, T.; Huang, B. Q.; Corbett, J. D.; Kanatzidis, M. G. *J. Solid State Chem.* **2000**, *153*, 321.
- (3) Kauzlarich, S. M.; Brown, S. R.; Snyder, G. J. *Dalton Trans.* **2007**, 2099.
- (4) Snyder, G. J.; Christensen, M.; Nishibori, E.; Caillat, T.; Iversen, B. B. *Nat. Mater.* **2004**, *3*, 458.
- (5) Snyder, G. J.; Toberer, E. S. *Nat. Mater.* **2008**, *7*, 105.
- (6) Slack, G. A., Rowe, D. M., Eds. *CRC Handbook of Thermoelectrics*; CRC Press: Boca Raton, FL, 1995.
- (7) Kim, S. J.; Hu, S. Q.; Uher, C.; Kanatzidis, M. G. *Chem. Mater.* **1999**, *11*, 3154.
- (8) Kim, S. J.; Kanatzidis, M. G. *Inorg. Chem.* **2001**, *40*, 3781.
- (9) Clarke, D. R. *Surf. Coat. Technol.* **2003**, *163*, 67.
- (10) Cordier, G.; Czech, E.; Jakowski, M.; Schäfer, H. *Rev. Chim. Miner.* **1981**, *18*, 9.
- (11) Cordier, G.; Schäfer, H.; Stelter, M. *Z. Naturforsch. B* **1985**, *40*, 5.
- (12) Cordier, G.; Stelter, M. *Z. Naturforsch. B* **1988**, *43*, 463.
- (13) Cordier, G.; Schäfer, H.; Stelter, M. *Z. Naturforsch. B* **1984**, *39*, 727.
- (14) Verdier, P.; l'Haridon, P.; Maunaye, M.; Laurent, Y. *Acta Crystallogr. B* **1976**, *32*, 726.
- (15) Kim, S. J.; Ireland, J. R.; Kannewurf, C. R.; Kanatzidis, M. G. *J. Solid State Chem.* **2000**, *155*, 55.
- (16) Park, S. M.; Choi, E. S.; Kang, W.; Kim, S. J. *J. Mater. Chem.* **2002**, *12*, 1839.
- (17) Verdier, P.; Maunaye, M.; Marchand, R.; Lang, J. C. *R. Seances Acad. Sci. Ser. C* **1975**, *281*, 457.
- (18) Cordier, G.; Savelsberg, G.; Schaefer, H. *Chem. Sci.* **1982**, *37*, 975.
- (19) Toberer, E. S.; Zevalkink, A.; Crisosto, N.; Snyder, G. J. *Adv. Funct. Mater.* **2010**, *20*, 4375.
- (20) Yan, Y. L.; Wang, Y. X. *J. Mater. Chem.* **2011**, *21*, 12497.
- (21) Yan, Y. L.; Wang, Y. X.; Zhang, G. B. *J. Mater. Chem.* **2012**, *22*, 20284.
- (22) Zevalkink, A.; Toberer, E. S.; Bleith, T.; Flage-Larsen, E.; Snyder, G. J. *J. Appl. Phys.* **2011**, *110*, 013721.
- (23) Zevalkink, A.; Swallow, J.; Snyder, G. J. *J. Electron. Mater.* **2012**, *41*, 813.
- (24) Zevalkink, A.; Pomrehn, G. S.; Johnson, S.; Swallow, J.; Gibbs, Z. M.; Snyder, G. J. *Chem. Mater.* **2012**, *24*, 2091.

- (25) Johnson, S. I.; Zevalkink, A.; Snyder, G. J. *J. Mater. Chem.* **2013**, *1*, 4244.
- (26) Todorov, I.; Chung, D. Y.; Ye, L. H.; Freeman, A. J.; Kanatzidis, M. G. *Inorg. Chem.* **2009**, *48*, 4768.
- (27) Fornasini, M. L.; Manfrinetti, P. Z. *Krist-New Cryst. St.* **2009**, *224*, 345.
- (28) SAINT; Bruker AXS: Madison, WI, 1999.
- (29) Sheldrick, G. M. S. *Empirical Absorption Correction Program*; University of Göttingen: Göttingen, Germany, 1997.
- (30) WinGX. A Windows Program for Crystal Structure Analysis: Farrugia, L. J. *J. Appl. Crystallogr.* **1999**, *32*, 837.
- (31) Sheldrick, G. M. *Acta Crystallogr.* **2008**, *A64*, 112.
- (32) SHELXTL, 5.10; Bruker Analytical X-ray Systems: Madison, WI, 1997.
- (33) Putz, H.; Brandenburg, K. *Diamond — Crystal and Molecular Structure Visualization*; Crystal Impact GbR: Bonn, Germany, 2011.
- (34) Blaha, P.; Schwarz, K.; Madsen, G. K. H.; Kvasnicka, D.; Luitz, J. *WIEN2k, An Augmented Plane Wave + Local Orbitals Program for Calculating Crystal Properties*; Technical University: Wien, Germany, 2001.
- (35) Perdew, P.; Burke, K.; Ernzerhof, M. *Phys. Rev. Lett.* **1996**, *77*, 3865.
- (36) Monkhorst, H. J.; Pack, J. D. *Phys. Rev. B* **1976**, *13*, 5188.
- (37) Sanderson, R. T. *J. Am. Chem. Soc.* **1983**, *105*, 2259.
- (38) Allen, F. H.; Kennard, O.; Watson, D. G.; Brammer, L.; Orpen, A. G.; Taylor, R. *J. Am. Chem. Soc.* **1987**, *2*, S1.
- (39) Smart, J. S. *Effective Field Theories of Magnetism*; Saunders: Philadelphia, PA, 1966.
- (40) Kittel, C. *Introduction to Solid State Physics*, 7th ed.; John Wiley and Sons: Hoboken, NJ, 1996.
- (41) Subbarao, U.; Peter, S. C. *Inorg. Chem.* **2012**, *51*, 6326.
- (42) Subbarao, U.; Gutmann, M. J.; Peter, S. C. *Inorg. Chem.* **2013**, *52*, 2219.
- (43) Subbarao, U.; Peter, S. C. *Cryst. Growth Des.* **2013**, *13*, 953.
- (44) Peter, S. C.; Chondroudi, M.; Malliakas, C. D.; Balasubramanian, M.; Kanatzidis, M. G. *J. Am. Chem. Soc.* **2011**, *133*, 13840.
- (45) Peter, S. C.; Rayaprol, S.; Francisco, M. C.; Kanatzidis, M. G. *Eur. J. Inorg. Chem.* **2011**, 3963.
- (46) Chondroudi, M.; Peter, S. C.; Malliakas, C. D.; Balasubramanian, M.; Li, Q. A.; Kanatzidis, M. G. *Inorg. Chem.* **2011**, *50*, 1184.
- (47) Peter, S. C.; Eckert, H.; Fehse, C.; Wright, J. P.; Attfield, J. P.; Johrendt, D.; Rayaprol, S.; Hoffmann, R. D.; Pottgen, R. *J. Solid State Chem.* **2006**, *179*, 2376.
- (48) Stockert, O.; Arndt, J.; Faulhaber, E.; Geibel, C.; Jeevan, H. S.; Kirchner, S.; Loewenhaupt, M.; Schmalzl, K.; Schmidt, W.; Si, Q.; Steglich, F. *Nat. Phys.* **2011**, *7*, 119.
- (49) Sengupta, K.; Sampathkumaran, E. V.; Nakano, T.; Hedo, M.; Abliz, M.; Fujiwara, N.; Uwatoko, Y.; Rayaprol, S.; Shigetoh, K.; Takabatake, T.; Doert, T.; Jemetio, J. P. F. *Phys. Rev. B* **2004**, *70*, 064406.
- (50) Sampathkumaran, E. V.; Ekino, T.; Ribeiro, R. A.; Sengupta, K.; Nakano, T.; Hedo, M.; Fujiwara, N.; Abliz, M.; Uwatoko, Y.; Rayaprol, S.; Doert, T.; Jemetio, J. P. F. *Physica B* **2005**, *359*, 108.
- (51) Kanchana, V.; Vaitheeswaran, G.; Zhang, X. X.; Ma, Y. M.; Svane, A.; Eriksson, O. *Phys. Rev. B* **2011**, *84*, 205135.
- (52) Svane, A.; Kanchana, V.; Vaitheeswaran, G.; Santi, G.; Temmerman, W. M.; Szotek, Z.; Strange, P.; Petit, L. *Phys. Rev. B* **2005**, *71*, 045119.
- (53) Vaitheeswaran, G.; Petit, L.; Svane, A.; Kanchana, V.; Rajagopalan, M. *J. Phys.: Condens. Matter* **2004**, *16*, 4429.